arXiv:2504.11901v2 [cs.RO] 17 Apr 2025

CAUSALITY-ENHANCED DECISION-MAKING FOR AUTONOMOUS MOBILE ROBOTS IN DYNAMIC ENVIRONMENTS

Luca Castri
University of Lincoln
lcastri@lincoln.ac.uk

Gloria Beraldo
National Research Council of Italy
University of Padua
gloria.beraldo@cnr.it

Nicola Bellotto
University of Padua
University of Lincoln
nbellotto@dei.unipd.it

ABSTRACT

The growing integration of robots in shared environments—such as warehouses, shopping centres, and hospitals—demands a deep understanding of the underlying dynamics and human behaviours, including how, when, and where individuals engage in various activities and interactions. This knowledge goes beyond simple correlation studies and requires a more comprehensive causal analysis. By leveraging causal inference to model cause-and-effect relationships, we can better anticipate critical environmental factors and enable autonomous robots to plan and execute tasks more effectively. To this end, we propose a novel causality-based decision-making framework that reasons over a learned causal model to predict battery usage and human obstructions, understanding how these factors could influence robot task execution. Such reasoning framework assists the robot in deciding when and how to complete a given task. To achieve this, we developed also PeopleFlow, a new Gazebo-based simulator designed to model context-sensitive human-robot spatial interactions in shared workspaces. PeopleFlow features realistic human and robot trajectories influenced by contextual factors such as time, environment layout, and robot state, and can simulate a large number of agents. While the simulator is general-purpose, in this paper we focus on a warehouse-like environment as a case study, where we conduct an extensive evaluation benchmarking our causal approach against a non-causal baseline. Our findings demonstrate the efficacy of the proposed solutions, highlighting how causal reasoning enables autonomous robots to operate more efficiently and safely in dynamic environments shared with humans.

***K*eywords** Causal Discovery and Inference, Robot Autonomy, Human-Robot Spatial Interaction, Decision-Making.

1 Introduction

Autonomous mobile robots are a game changer for the progress and development of various sectors, including industry, logistics, agriculture, and healthcare. However, operating in dynamic environments and workspaces shared with people introduces several challenges. In particular, unexpected events and human encounters can negatively affect the capacity of a robot to fulfill its task safely and autonomously. Understanding the causal effect of the robot's actions enables it to better assess and choose them, which is crucial for improving both the efficiency and safety of its operations. This motivates the need for intelligent solutions to reason about the causal relationships between the environment and human-robot interactions, improving robot's efficiency and guaranteeing human safety. Unsurprisingly, the importance of cause-and-effect reasoning in AI and robotics has become strategically important for national and international research programmes[1,2][1, 2].

Knowing the causal structure of a system provides a significant advantage in many robotics applications. Indeed, research in causal inference, which includes causal *discovery* and *reasoning*, has gained increasing attention in recent robotics literature [3, 4, 5, 6, 7, 8, 9, 10, 11, 12, 13, 14, 15]. However, to the best of our knowledge, no prior work

[1]euRobotics, "A Unified Vision for European Robotics", https://eu-robotics.net/strategy/

[2]National Robotics Initiative 3.0, "Innovations in Integration of Robotics", https://www.nsf.gov/pubs/2021/nsf21559/nsf21559.htm

has explored causal inference for robot decision-making in the context of dynamic environments and human-aware navigation. The latter in particular typically relies on predictive models of human motion, which are often reactive and do not take into account robot and human goals, or how contextual factors can influence them. As a result, autonomous robot navigation in these environments can lead to potential safety and efficiency issues.

Consider for example a mobile robot in a warehouse shared with humans, as depicted in Fig. 1. The robot must reach a target location while accounting for how humans behave within the shared space, considering the layout of the environment and other contextual factors, such as the time of day. Discovering the cause-and-effect relationships among these factors enables the robot to reason about them, making it aware of the mechanisms driving human behaviour and allowing it to make decisions based on causal knowledge. As shown in Fig. 1, thanks to its causal model the robot infers that, although the path through the canteen is longer than the direct route through the working area, it is the safest and most efficient option *because* it is not lunchtime and the canteen is less crowded. By choosing this path, the robot can efficiently reach its target position, minimising the number of unexpected obstacles and the risk of collisions with humans.

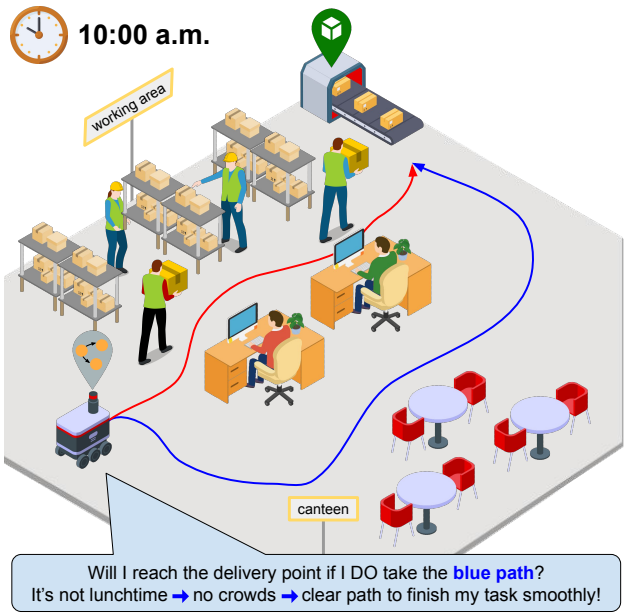

Figure 1: A mobile robot reasoning on the causal model of human spatial behaviours in a warehouse environment to navigate safely and efficiently.

This paper presents a causality-enhanced decision-making framework to model relevant robot and human states within a shared workspace, enabling causal reasoning that improves task-execution efficiency and safety. We demonstrate that with our framework a mobile robot can reconstruct the underlying causal relationships between autonomous navigation, human spatial behaviour, and surrounding environment from data. By leveraging this knowledge, it can efficiently complete its tasks while ensuring that human-robot spatial interactions (HRSIs) remain as safe as possible. In summary, our contributions are as follows:

- a novel causal inference framework for robotic decision-making, integrated within the Robot Operating System (ROS), to improve task-execution efficiency and safety in dynamic human-shared environments;
- a new Gazebo-based simulator, called PeopleFlow[3], which generates complex human and robot spatial behaviours considering various contextual factors (e.g., dynamic changes based on different goals and times of the day), as shown in Fig. 1;
- a thorough experimental evaluation of the causal framework in a complex warehouse simulation to demonstrate its feasibility and potential for real-world robotic applications.

PeopleFlow is available as a Docker image on GitHub: `https://github.com/lcastri/PeopleFlow`.

The paper is structured as follows: basic concepts about causal discovery and related work in the robotics fields are presented in Section 2; Sections 3 and 4 explains the details of our causality-based decision making framework and PeopleFlow; Section 5 presents the application and results of our approach in a simulated warehouse-like environment; Section 6 justifies the choice of causality over standard Bayesian inference; finally, Section 7 concludes the paper discussing achievements and future work.

2 Related Work

The synergy between causality and robotics offers mutual benefits. Causality leverages robots' physical capabilities for interventions, while robots utilise causal models to gain a deeper understanding of their environment. This synergy has led to increased attention towards causal inference in various robotics applications. Causal inference comprises two main phases: causal discovery and causal reasoning.

[3]PeopleFlow GitHub repository: `https://github.com/lcastri/PeopleFlow`

Causal Discovery in Robotics: Causal discovery involves identifying the underlying causal structure from data, either through observational methods, interventional experiments, or a combination of both. It aims to uncover cause-and-effect relationships between variables rather than mere correlations. Numerous methods have been developed for causal discovery from both static and time-series data [16, 17]. However, for robotics applications, where time-series sensor data is common, methods tailored specifically for time-dependent causal discovery are essential. Among the various approaches available in the literature, the time-series variation of the Peter and Clark (PC) [18] algorithm, such as PC Momentary Conditional Independence (PCMCI) [19], has been widely used in many applications, including robotics [20, 21, 6]. PCMCI has recently been extended with several enhancements. PCMCI$^+$ [22] enables the discovery of simultaneous dependencies. Filtered-PCMCI (F-PCMCI) [7] integrates a transfer entropy-based feature-selection module to improve causal discovery by focusing on relevant variables. Joint-PCMCI$^+$ (J-PCMCI$^+$) [23] supports causal structure learning from multiple observational datasets using context variables. Latent-PCMCI (LPCMCI) [24] allows causal discovery in the presence of latent confounders. CAnDOIT [25], which stands for Causal Discovery with Observational and Interventional Data from Time Series, extends LPCMCI by integrating both observational and interventional data for improved causal discovery. Additionally, PCMCI and F-PCMCI have been integrated into a ROS-based causal discovery framework, ROS-Causal [26], facilitating their applicability in robotic systems.

Causal Reasoning in Robotics: Once the causal structure is established, causal reasoning enables inference, prediction, and decision-making by leveraging the discovered causal relationships to estimate the values of variables within the causal model, assess the effects of interventions, and evaluate counterfactual scenarios. Structural Causal Models (SCMs) have been employed to understand how humanoid robots interact with tools [4]. PCMCI and F-PCMCI have been used to establish causal models for underwater robots navigating toward target positions [5] and to predict human spatial interactions in social robotics [6, 7]. Moreover, causality-based approaches have been explored in various robotics domains, including robot imitation learning, manipulation and explainable HRI [8, 9, 10, 14, 15].

Despite the growing use of causality in robotics, most existing approaches primarily focus on causal discovery and the prediction of time-series variables within the causal model. While some recent works [11, 12, 13] have explored causal reasoning for robot manipulation tasks, drone applications and planning, the use of causal models for decision-making in human-centered environments remains largely unexplored. In contrast, our work focuses on integrating causal reasoning into the robot's decision-making process in dynamic environments shared with humans. By leveraging causal inference, our framework enables robots to make causality-aware decisions, enhancing both task execution efficiency and human safety in HRSI scenarios.

Human Robot Spatial Interaction: Several studies have highlighted the importance of considering the coexistence of humans and robots in shared environment, whether they are collaborating or performing individual tasks [27, 28, 29]. In this work, we focus on the spatial aspect of the interactions between human-human, human-robot and human-object [30]. Recently, various methods have been proposed to model the relations between human motion behaviours and spatial interactions [31, 32, 33]. However, these approaches have not explicitly considered causal relationships between spatial variables. Some recent studies [34, 6, 7] have developed causal models for modelling HRSI.

Despite these advances, none of the existing works explicitly account for contextual factors—such as the influence of surrounding agents, dynamic environmental conditions, and task-specific constraints—when modelling HRSIs. These factors can alter the relationships between variables, causing interactions to strengthen, weaken, or even emerge or disappear depending on the specific context in which the system is observed. Analysing these dependencies requires diverse datasets covering various environments, agent behaviors, and tasks, but such data are currently unavailable. Collecting them across all possible conditions would be impractical and highly time-consuming.

Most existing datasets primarily focus on human motion trajectories rather than capturing how contextual elements shape human-robot interactions. For instance, THÖR [35] and its extension THÖR-MAGNI [36] provide motion trajectories recorded in controlled indoor environments using ceiling-mounted cameras, while the ATC Pedestrian Tracking dataset [37] tracks pedestrians in a shopping mall atrium using 3D range sensors. Similarly, the JackRabbot Dataset and Benchmark (JRDB) [38] captures human poses from a mobile robot's ego-perspective using RGB cameras and 3D LiDAR. While these datasets offer valuable insights into human motion patterns, they do not include contextual variability, such as how different environmental settings, external agents, or task constraints influence interaction dynamics.

To address this limitation, simulation environments offer a practical solution for generating diverse, controlled, and repeatable HRSI scenarios. By systematically varying contextual factors, simulators enable the exploration of how different conditions influence human-robot interactions, effectively filling the gap left by existing datasets. SEAN 2.0 [39] provides a high-fidelity, Unity-based simulation environment tailored for pedestrian interactions, making it well-suited for training vision-based robotics algorithms in dynamic social settings. In contrast, MengeROS [40], CrowdNav [41], and SocialGym [42] focus on 2D grid-based visualisations, which, while useful for algorithmic benchmarking, may

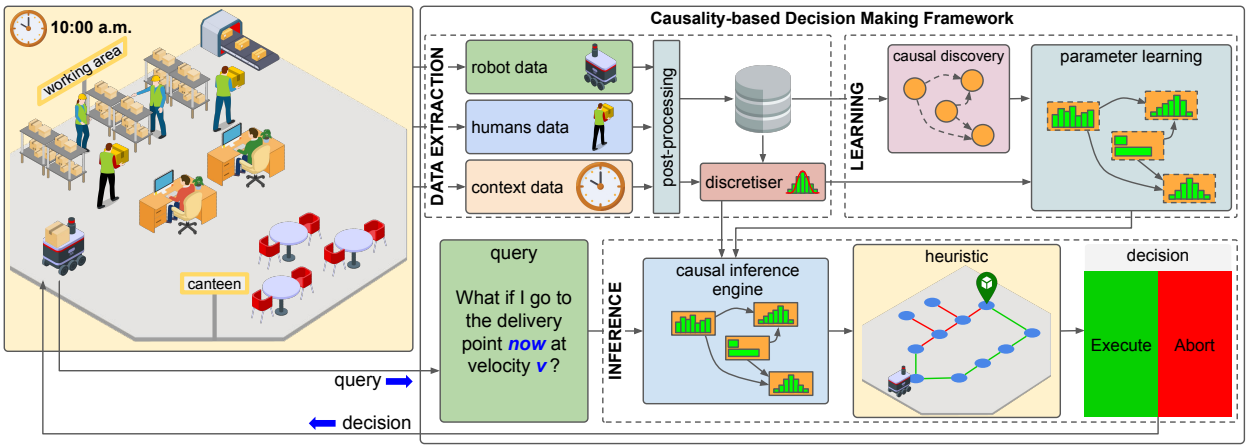

Figure 2: Block scheme of the causality-based decision making framework, consisting of three main pipelines: *(i) Data Extraction* which gathers and preprocesses data from the observed scenario; *(ii) Learning* that retrieves the causal model describing the observed scenario and exploits its structure along with extracted data to learn the parameters of the causal inference engine; *(iii) Inference*, which uses the learnt causal inference engine to estimate relevant quantities for determining a path to complete a task and deciding in advance whether execute it or abort it.

lack the realism needed to model complex human behaviours in rich environments. ROS-Causal_HRISim[4] [26] takes a different approach by enabling causal analysis in HRI scenarios, allowing both observational data collection and targeted interventions involving humans and robots.

Our new Gazebo-based simulator, PeopleFlow, builds upon ROS-Causal_HRISim to support context-sensitive human-robot spatial interactions. Unlike existing simulators, it does not only record HRSI data across diverse contexts but also models and dynamically assigns the roles of humans and robots based on probabilistic distributions conditioned on the context. This enhanced simulation framework offers the ability to record HRSI data across different contextual scenarios, in which people and robot have a role that depends on the context, enabling a more comprehensive analysis of how environmental conditions, agent behaviours, and task constraints influence human-robot interactions.

3 Causality-based Robot Decision Making Framework

Our approach aims to develop a *causal inference engine* [43] to enable causal reasoning in robotic decision-making. Specifically, we propose a framework that allows a robot to determine a path for completing a given task (e.g., delivering an object to a designated location) that represents a trade-off between factors relevant in its operating environment. These factors may include the current situation of the environment (e.g. people crowding an area at a specific time) or a robot-related constraint, such as battery level, that could influence task execution. Additionally, the framework should be capable of preemptively deciding whether to initiate or abort a task to avoid failures or inefficiencies.

Deciding which path to take to reach a destination allows the robot to operate more efficiently while ensuring human-robot interactions remain as safe as possible. For instance, consider a scenario, shown in Fig. 1, where the robot is in a warehouse environment shared with people and needs to travel from its current position to the delivery point, with two possible paths. The first route (red path in Fig. 1) is the shortest but also the busiest, meaning the robot may need to spend significant time and energy navigating around people, increasing both the risk of collisions and battery consumption. In contrast, the second route is longer but completely clear (blue path in Fig. 1). Despite being physically longer, this second path could enable the robot to reach its destination more safely, more quickly and with lower battery consumption since it avoids people.

Building our framework involves multiple steps, which can be broadly categorised into three main blocks: *data extraction*, *learning*, and *inference*, as illustrated in Fig. 2.

[4] `https://github.com/lcastri/ROS-Causal_HRISim`

3.1 Data Extraction Pipeline

The *data extraction* phase is the first block of our framework, providing input to the learning and inference components. This phase is responsible for the continuous extraction of data from the observed scenario, capturing information related to the robot, humans, and contextual factors.

For the learning pipeline, the data must be preprocessed to facilitate the discovery of the causal model and the construction of the causal inference engine. The first step in this process is subsampling. Given the large volume of collected data, subsampling is applied to reduce the dataset size while preserving essential information. This step ensures that the dataset remains computationally manageable without compromising the integrity of the data distribution. Since our dataset consists of multiple time-series, we determine the appropriate subsampling rate based on the Nyquist-Shannon sampling theorem to prevent information loss. Specifically, we first analyse the spectral content of each time-series to identify its highest frequency component (bandwidth BW_{max}) and then set the subsampling rate as $f_s \geq 2 \cdot BW_{\text{max}}$ where f_s is the subsampling frequency and BW_{max} is the highest significant frequency present in the dataset. This ensures that the subsampled data retains all relevant dynamics.

Next, the data undergoes post-processing to extract relevant time-series information from the raw collected data, which is then stored for causal discovery analysis. To construct the causal inference engine, the extracted data must be compatible with inference mechanisms that often rely on discrete data representations. Therefore, we apply a discretisation step using pyAgrum[5]'s built-in discretiser to transform continuous variables into discrete states while preserving essential statistical properties. Specifically, we use the *quantile* [44] and *elbow method* [45] approaches for discretisation. The quantile approach is particularly suitable when data is skewed or non-uniformly distributed, as in our case, whereas the elbow method helps to automatically determine the number of bins per variable.

Once the dataset has been processed, it is ready to be fed into the learning and the inference pipelines (see Fig. 2). For the latter, the data is continuously captured and post-processed as described above. However, in this case, the data is not stored but instead discretised and directly used for real-time inference. In the following sections, we provide a more detailed explanation of the learning and inference pipelines.

3.2 Learning Pipeline

The *learning* phase comprises both causal discovery and parameters learning. It first focuses on uncovering the underlying causal relationships governing human and robot behaviours in the working environment. Once the causal structure is identified, the model's parameters are estimated to enable reasoning over the retrieved causal relationships.

As previously explained, the causal discovery block takes as input the post-processed information from the data pipeline and performs the causal analysis to uncover the underlying causal structure governing the observed scenario. The analysis is conducted using CausalFlow[6], a Python library that provides a collection of methods for causal discovery from time-series, as reviewed in Sec. 2. Embedding CausalFlow into our framework makes it adaptable to various scenarios. The choice of the causal discovery method depends on the dataset characteristics. For basic causal discovery, approaches such as PCMCI, DYNOTEARS, and VARLiNGAM can be applied. When the dataset requires feature selection, F-PCMCI is used, whereas L-PCMCI is more suitable when latent variables are present. If the dataset contains a mix of observational and interventional data, CAnDOIT is the appropriate method. In our case, since our dataset contains contextual variables, we use J-PCMCI$^+$ [23].

Inspired by [46], the causal structure derived in the previous block is used together with the discretised data to learn the parameters of the causal inference engine. For this, we again employ pyAgrum[5] for estimating the conditional probability distributions associated with each node in the causal graph, ensuring consistency with the causal structure identified in the discovery step. Unlike the approach in [46], which employs the Expectation-Maximization (EM) algorithm, we use Maximum Likelihood Estimation (MLE) [47], as our dataset does not contain missing data. These steps form the *learning pipeline* and are shown in Fig. 2.

3.3 Inference Pipeline

Once built, the causal inference engine can be used by the robot to make decisions based on inferred information. Specifically, the *inference pipeline* begins with a query from the robot at the start of an assigned task. Before proceeding, the robot must first gather information that is crucial for successfully accomplishing the task. As previously mentioned, this information can be related to the environment in which the robot operates or to its internal state, both of which influence task completion.

[5] `https://pyagrum.readthedocs.io/en/1.17.2/`

[6] `https://github.com/lcastri/causalflow`

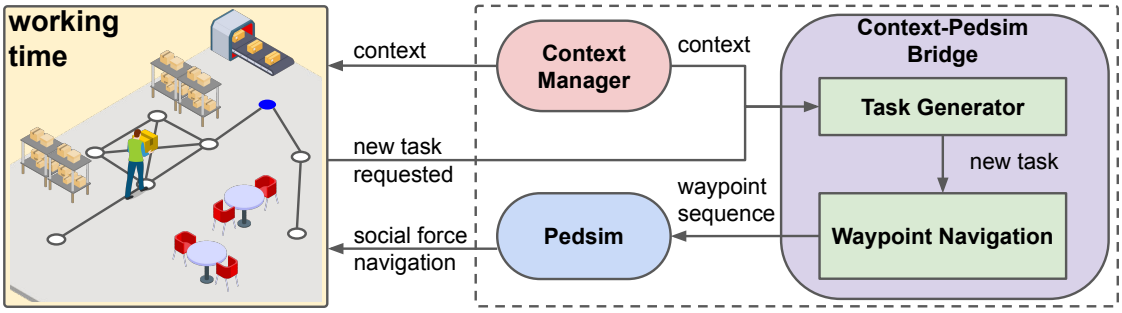

Figure 3: Overview of PeopleFlow's context-aware agent behaviour strategy. The Context Manager node handles the contextual factors—in this example, time. After the agent picks up a box from a shelf, it requests a new task. The Context-Pedsim Bridge node receives the task request and generates a new task for the agent depending on the current context. Since it is working-time, the agent is tasked to bring the box to the delivery point. A corresponding sequence of waypoints is generated and passed to Pedsim, which navigates the agent to the goal using the social force model. The agent's goal is marked with a blue circle, while white circles represent the remaining waypoints.

The robot's query is formulated as an intervention, representing an action it considers taking to accomplish the task (e.g., *What if I do(X)?*). Through the causal inference engine, which has been previously learnt, the inference pipeline evaluates the potential consequences of this action by estimating how relevant factors would change as a result of an intervention or condition. The output of this process is the conditional probability distribution of the queried factor, taking into account causal links within the causal model. Once again, this inference step is performed using pyAgrum[5], which provides a full implementation of do-calculus [48] for this step [49]. The estimated value of the factor is then obtained by computing its expectation over the inferred probability distribution. The estimated value is finally embedded in a heuristic used by the A* algorithm to define the robot's path. If a valid path is found under certain conditions, the inference pipeline returns a decision to proceed with the task using the selected path. In contrast, if no valid path is found, an abort signal is returned to the robot. These steps constitute the *inference pipeline* and are shown in Fig. 2. A use-case implementation of the framework is presented in the following section, including an example of causal inference for decision making in Sec. 4.3.

4 Simulating Contextual Human-Robot Spatial Interactions

To address the limitations of existing datasets and simulators, which overlook contextual dependencies in HRSI, we introduce *PeopleFlow*, a simulation framework designed to capture and model context-sensitive behaviours in human-robot and human-human interactions.

PeopleFlow enables the creation of realistic, diverse, and repeatable spatial interaction scenarios by incorporating contextual factors that dynamically influence human and robot behaviours. These contextual factors—such as time, location, and environmental obstacles—are crucial in shaping the interactions dynamic. In addition, as highlighted in previous work [26, 50], such simulation environments not only support data generation but also provide a controlled setting for verifying the correctness of causal models and evaluating the experimental procedures used to extract them. This helps reduce both time wasted on ineffective experiments and unnecessary financial costs.

4.1 PeopleFlow

We developed PeopleFlow by building upon our previous work[4][26]. The latter is a Gazebo-based simulator to support causal inference in HRSI scenarios, enabling the collection of observational data and allowing for interventions involving both the robot and humans. PeopleFlow is designed for modelling human-human and human-robot spatial interactions in shared workspaces. Its key novelty lies in contextualising agent behaviours—both for humans and robots—based on scenario-specific factors such as time-dependent routines, robot states, and dynamic environmental conditions, all of which influence interaction patterns. The simulator is built on Gazebo and ROS and features a TIAGo[7] robot alongside multiple pedestrian agents. Human behaviour is modelled using the *pedsim_ros*[8] library, which simulates group and individual movements based on a social force model [51]. On top of this simulation stack, we introduce two new ROS nodes: the *Context Manager* and the *Context-Pedsim Bridge*.

[7] `https://pal-robotics.com/robot/tiago/`
[8] `https://github.com/srl-freiburg/pedsim_ros`

The Context Manager node governs the scenario-specific contextual factors (e.g. time-dependent routines) and communicates the current context to the Context-Pedsim bridge node. The Context-Pedsim Bridge handles the generation of new tasks for pedestrian agents and computes their navigation plans accordingly. In more details, we introduced a waypoint-based division of the environment into meaningful regions, such as workspaces, canteens, offices, and corridors. These waypoints serve both as semantic labels and as navigation nodes for guiding agent movement. Their connectivity is defined based on their spatial arrangement while ensuring that direct paths between them do not intersect obstacles or fall within the influence radius of other waypoints. When an agent requests a new task, the Context-Pedsim Bridge node, based on the current context, selects a destination waypoint (i.e., an activity station) and assigns a random activity duration. The agent's current position and assigned destination are then passed to an A*-based path planner, which computes the shortest waypoint sequence to reach the goal. Once the agent reaches the destination, it remains stationary for the designated time to simulate engagement in the activity. Afterward, the task cycle restarts. The whole strategy is shown in Fig. 3. Mapping destinations to specific waypoints and driving task assignment based on contextual rules (e.g., time of day), enables the production of more realistic and interpretable human activities.

Our simulator is designed to be modular, extensible and adaptable to different kinds of shared environments, contextual factors, and task structures. A Docker image of PeopleFlow is publicly available on GitHub[3].

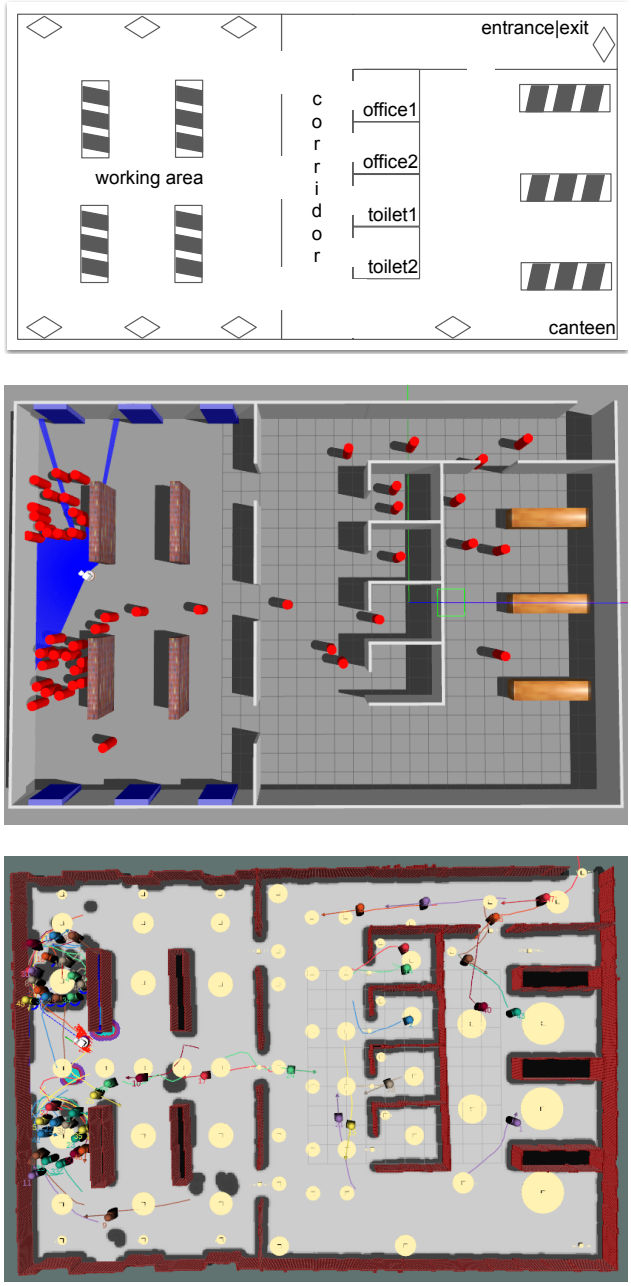

Figure 4: (Top) Warehouse-like scenario map with obstacles depicted as black-band rectlangles, and robot target stations as diamonds. Its implementation in our simulator: (Centre) Gazebo view, (Bottom) RViz view.

4.2 Context-sensitive Humans and Robot Behaviours in a Warehouse Setting

In this paper, we focus on a warehouse-like scenario—based on our funding project DARKO[9] and common industrial settings [52]—as a case study to evaluate our causality-based robot decision-making framework. Fig. 4 (top) illustrates the map of the warehouse environment implemented in our simulator. The environment consists of several main areas, including the entrance, two offices, two toilets, a canteen, a working area, and a corridor connecting all these spaces. Black-band rectangles indicate shelves in the working area where humans perform tasks and tables in the canteen, while diamonds represent target points for the robot (e.g., trays and conveyors). In Gazebo (Fig. 4, centre), humans are represented as red cylinders, whereas in RViz (Fig. 4, bottom), they are visualised as manikins. We now describe the contextual factors, robot features, and how we modelled worker activities within this environment.

4.2.1 Contextual Factors

We model key contextual factors that affect both human and robot behaviours, as well as their interaction in a warehouse scenario:

[9] `https://darko-project.eu/`

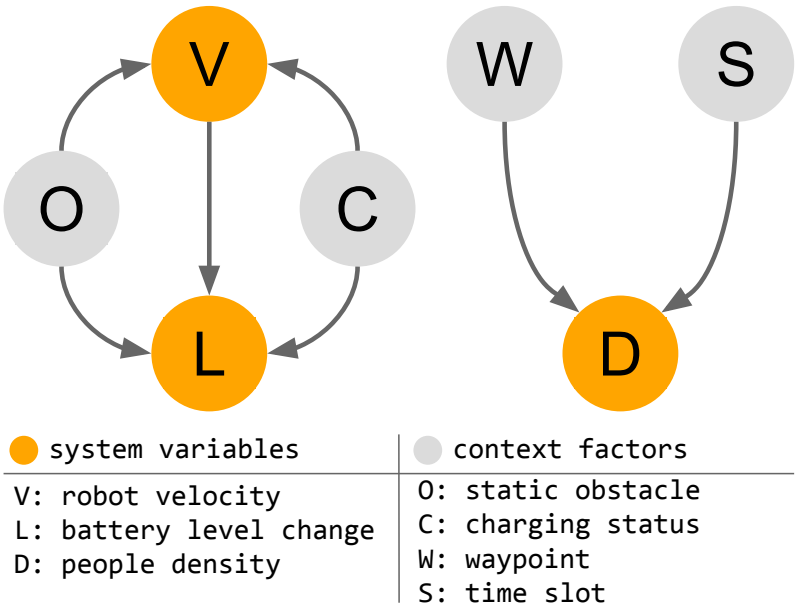

Figure 5: Causal model of the scenario staged by PeopleFlow. Contextual factors W, S, C, and O are shown in grey, while system variables V, L, and D are highlighted in orange.

- *Waypoint* (W), which identifies a specific area of the warehouse environment;
- *Time slot* (S), which affects human activities and robot task execution, simulating different operational dynamics throughout a typical warehouse shift;
- *Robot charging status* (C), distinguishing between scenarios where the robot is actively navigating or stationary at a charging station;
- *Presence of static obstacle* (O), which models the presence of obstacles not included in the map of the environment (e.g., a forklift or a box left by a human). This factor affects robot velocity and battery consumption, as they require additional maneuvers.

4.2.2 Robot Features

Autonomy is a key factor for any mobile robot operating in real-world environments. Among the many aspects that influence autonomy, battery life is crucial, as it directly affects the robot's ability to perform tasks and activities. In our simulator, we model battery dynamics, including both charging and discharging processes, to better approximate real-world conditions. Additionally, we model how the presence of an unexpected static obstacle in the environment affects the robot's battery dynamics and velocity. This allows us to more realistically simulate the robot's operation in a warehouse environment, where battery consumption is a critical factor that must be considered in the decision-making process [53, 54, 55, 56].

We model the battery level's change (L) based on two contextual factors: the charging status (C) and the presence of an unexpected static obstacle (O). Inspired by previous works [57], the battery dynamic in discharging mode ($C = 0$) is based on two primary factors: *static* and *dynamic* consumption. Static battery consumption accounts for energy usage when the robot is idle, primarily due to active sensors and other essential components. In contrast, dynamic battery consumption represents the energy expended due to the robot's movement. However, battery consumption increases in situations where the robot is forced to stop suddenly or perform maneuvers to avoid an unexpected static obstacle in the environment. Instead, when the robot is in charging mode, the battery level increases at a predefined charging rate. To capture these factors, we model the change in battery level over time using the following equation:

$$L_t = \begin{cases} -\Delta_t\Big(K_s + K_d \cdot V_t\Big) & C = 0, O = 0 \\ -\Delta_t\Big(K_s + K_d \cdot V_t\Big)K_o & C = 0, O = 1 \\ +\Delta_t \cdot K_c & C = 1 \end{cases} \tag{1}$$

where L_t represents the battery level's change at time step t, Δ_t is the time step duration, K_s is a constant representing static battery consumption, K_d is a coefficient related to battery consumption due to motion, V_t is the robot's velocity at

time step t, K_o is a coefficient representing the increase in battery consumption caused by static obstacles that force the robot to modify its behaviour unexpectedly. K_c is the charging rate when the robot is in charging mode. The two contextual factors, C and O, indicate the robot's charging status and the presence of a static obstacle, respectively. C is 0 when the robot is discharging and 1 when it is charging, while O is 0 when no obstacle is present and 1 when an obstacle is detected.

Thus, the battery level at time t is updated as follows:

$$B_t = B_{t-1} + L_{t-1} \tag{2}$$

where B_t and B_{t-1} denote the battery percentage at time t and $t-1$ respectively, and L_{t-1} represents the battery level's change, as modelled by (1), at time $t-1$.

By incorporating battery dynamics into the simulation, we account for the impact of its consumption and recharging needs on the robot's operation. This enables more realistic decision-making, such as determining whether to continue or abort a task based on battery levels, planning charging station visits, and selecting a navigation path that balances safety, time efficiency, and battery consumption.

The expected causal relationships between the mentioned factors derive from the model in (1) and are as follows:

- $L \leftarrow O \rightarrow V$: L is affected by O. Moreover, O influences V because the robot is forced to stop or maintain a low velocity when encountering an unexpected obstacle.
- $L \leftarrow C \rightarrow V$: When $C = 0$, L is discharging, whereas when $C = 1$, L is charging. Furthermore, $C = 1$ also forces the robot to remain stationary at the charging station, meaning $V = 0$.
- $V \rightarrow L$: The robot's velocity affects the battery change L in discharging mode.

Although we use time-series data, we omit explicit time indices t and $t-1$ for simplicity, as all the described links represent contemporaneous relationships occurring at time t. The considered relationships are illustrated by the Directed Acyclic Graph (DAG) in Fig. 5.

4.2.3 Worker Activities

In a warehouse, workers are assigned specific tasks at different times of the day. The activities assigned to each person are generally the same every day [58]. For instance, warehouse operators may be responsible for unloading goods in the morning, sorting and shelving items during the day, and preparing shipments in the evening. These tasks are generally repeated every working day. As a result, certain areas of the warehouse experience higher worker traffic during specific time periods, creating congestion zones.

In order to model this phenomenon, we divided the environment into distinct areas (waypoints) and introduced time as a contextual factor to differentiate workers' activities at different times of the day. Each waypoint represents a specific area of the warehouse that experiences varying levels of congestion depending on the time, making it an essential contextual factor in our model. To capture the temporal dynamics of workers activity, we divided the working period into hourly time slots from 08:00 to 18:00, along with an additional off period. Within each time slot, worker activities are predefined and consistent, reflecting the structured nature of warehouse operations. The 08:00–09:00 slot models workers' arrival and the beginning of the working day. To enhance realism, we model each worker arriving at a random time within this slot before starting their assigned activity. Time slots from 09:00 to 13:00 represent the normal morning working period, during which workers are typically present in operational areas such as shelves and offices. The 13:00–14:00 slot represents the lunch break, where workers are primarily in the canteen area. Following this, time slots from 14:00 to 18:00 model the afternoon working period, with the 17:00–18:00 slot representing the end of the working day, when workers finish their tasks and leave the warehouse after completing their standard eight-hour shift. After 18:00, we model the off period, during which no workers are present in the warehouse.

An example of a congestion zone in two different time slots is illustrated in Fig. 6. Based on this, we defined a variable called *people density* (D) to quantify the number of people in a specific waypoint. For each waypoint W in the set of waypoints Ω, the density D is defined as follows:

$$D = \frac{\text{Number of people in } W}{\pi \cdot r_W^2} \tag{3}$$

where r_W is the radius of the waypoint W.

By incorporating both waypoints and time slots as contextual factors, our model effectively represents fluctuating congestion levels within the warehouse. This enables a more accurate simulation of human-robot interactions, where robot navigation decisions account for dynamically changing environmental conditions. Following this, the causal

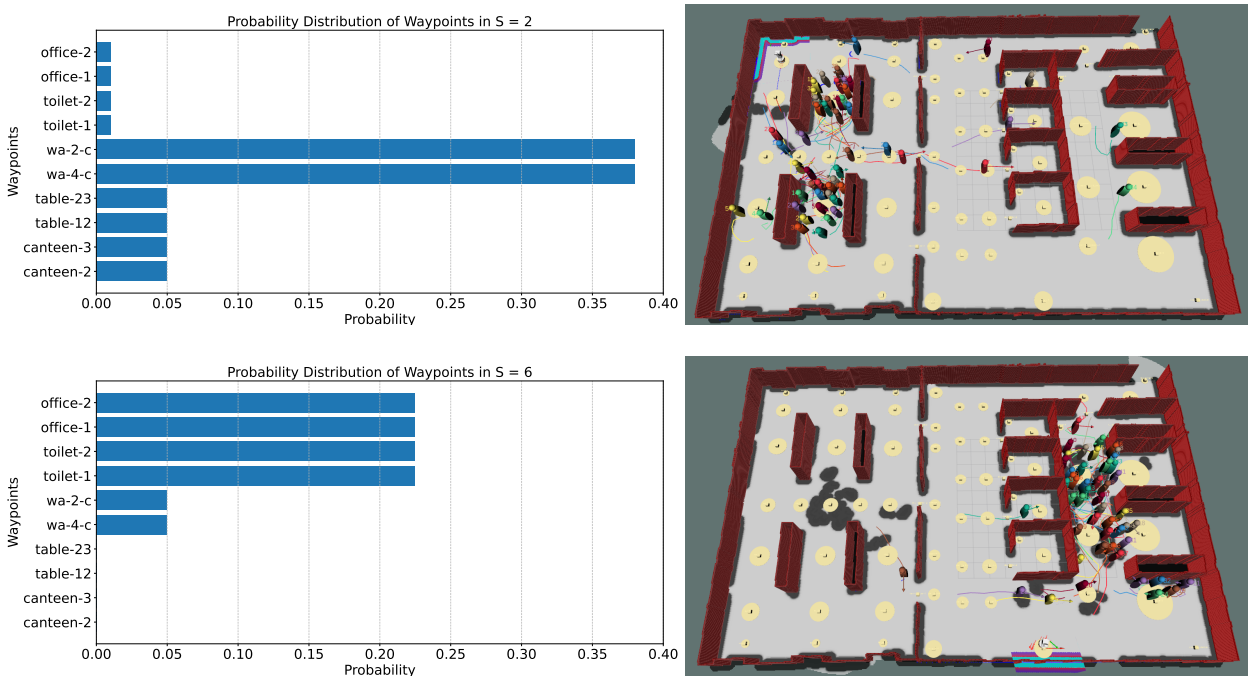

Figure 6: Two examples of people congestion areas at different time slots. (Top left) Probability distribution of waypoint choices for people in time slot 2 (09:00–10:00). (Top right) RViz view showing people primarily concentrated at the waypoints with the highest probabilities from the distribution graph. (Bottom left) Probability distribution of waypoint choices for people during lunchtime ($S6$, 13:00–14:00). (Bottom right) RViz view showing the majority of workers gathered in the canteen area.

influence from the contextual factors time slot S and waypoint W on the people density is $W \rightarrow D \leftarrow S$. Again, for simplicity, we have omitted the explicit time indices t and $t-1$. The latter causal relations are added to the model in Fig. 5.

4.3 Causality-based Robot Decision Making in PeopleFlow

Our causality-based decision making framework presented in Sec. 3.3 is a general causal inference approach adaptable to various scenarios. Here, we give more details on the factors that we want to infer with it and how they are used in the A* algorithm to decide whether to execute or not a given task, and in case to determine the best path.

Causal Inference Given the robot and workers features extracted from the simulator, as well as the context factors explained in Sec. 4.2.1, the crucial aspects affecting robot task completion are the robot battery consumption L and the people density D in specific areas of the environment. Given their dependencies with other variables and/or contextual factors, the robot can infer L based on its velocity V and charging status C, while D can be estimated using the specific time slot S and waypoint W. These inferences are made under the assumption that the robot has knowledge of its own velocity and charging status. Additionally, in a warehouse shared with workers, we assume that the robot is aware of the current time, enabling it to determine S, as well as the predefined waypoints in the environment.

For instance, consider a scenario where the robot is assigned the task "transport an object to the delivery point", as depicted in Fig. 2. To determine in advance whether the task can be successfully completed or if it should be immediately refused, the robot poses the following query:

"What if I go to the delivery point now at velocity v?"

This query involves two causal interventions: one on the time ("now") and another on the velocity (v). These interventions are essential for estimating L and D, allowing the robot to make an informed decision about whether to proceed with the task. Specifically, the robot can query the causal inference engine to estimate the following probability distributions:

$$\mathrm{P}(L = l \mid do(V = v), C = c) \quad \forall l \in \Gamma \tag{4}$$

$$\mathrm{P}(D = d \mid do(S = s), W = w) \quad \forall d \in \Psi, \forall w \in \Omega \tag{5}$$

where Γ and Ψ denote the sets of possible discretised values for L and D, respectively, and Ω is the set of waypoints. Eqs. (4) and (5) return the probability distribution of L and D, respectively, given the intervention and conditioning variables. These probability distributions are then used to retrieve the expected L and D as follows:

$$\hat{L} = \mathbb{E}[L \mid do(V = v), C = c] \tag{6}$$

$$\hat{D} = \mathbb{E}[D \mid do(S = s), W = w] \quad \forall w \in \Omega \tag{7}$$

To clarify, the robot queries the causal inference engine to determine whether it can start the task at the current S and travel at velocity v. Hence, for each waypoint in Ω, these two interventions allow the causal inference engine to estimate the expected values of L and D, which represent the cost associated with the specific waypoint in terms of battery consumption and the risk of encountering people or getting stuck, respectively. These quantities are then used as cost components for navigation planning. In particular, the battery cost for traversing an arc between two waypoints is first computed by determining the traversal time, which is the distance between the waypoints divided by the velocity v (used in the intervention). This duration is then multiplied by the expected $\hat{L}$ from Eq. (6), which corresponds to the battery consumption per time step when moving at velocity v. The result is the expected battery cost for that arc. These estimated values, along with the distance between waypoints, are finally used in a heuristic function defined below.

Heuristic Given a path $\pi = \{w_1, w_2, ..., w_n\}$ from the starting waypoint w_1 to the destination w_n, the A* algorithm evaluates paths using the standard cost function:

$$f(w_i) = g(w_i) + h(w_i) \tag{8}$$

where $g(w_i)$ represents the cumulative cost from the start node w_1 to the current node w_i, while $h(w_i)$ is the heuristic estimate of the remaining cost from w_i to w_n. For our problem, we define the heuristic cost function as:

$$\begin{aligned} h(w_i) = \sum_{i=1}^{n-1} \Big(& \lambda_D \cdot \delta(w_i, w_{i+1}) + \lambda_D \cdot \hat{D}(w_i) + \\ & + \lambda_L \cdot |\hat{L}(w_i, w_{i+1})| \Big) \end{aligned} \tag{9}$$

where $\delta(w_i, w_{i+1})$ represents the Euclidean distance between two consecutive waypoints, $\hat{D}(w_i)$ is the expected people density at waypoint w_i from the causal inference engine, $\hat{L}(w_i, w_{i+1})$ is the expected battery consumption to reach waypoint w_{i+1} from w_i, and $\lambda_D, \lambda_D, \lambda_L$ are weighting coefficients that balance the trade-off between distance minimisation, congestion avoidance, and battery efficiency.

Decision Making As already mentioned, we want the causal inference engine to be able not only to choose the path but also to determine whether the task should be executed. This decision must be based on the cumulative battery cost along the path π, defined as:

$$C_L(\pi) = \sum_{i=1}^{n-1} |L(w_i, w_{i+1})| \tag{10}$$

and a minimum battery threshold (B_{min}), a common safeguard in robotics to prevent critical failures. If the battery level falls below this threshold, the robot typically returns to the charging station or deactivates some power-consuming services. For instance, the TIAGo robot disables its arm motors, making manipulation tasks not possible. More specifically, if the remaining battery $B_t - C_L(\pi)$ after a candidate path π would fall below a threshold B_{min}, the path π must be discarded. This heuristic function (9) is integrated into Eq. 8 and guides the A* algorithm to expand paths from the starting waypoint to the destination, while minimising the total estimated cost along the path π. The heuristic function ensures that selected paths balance distance, congestion avoidance, and battery efficiency within the minimum battery constraint. If the A* finds a path that satisfies such constraint, the decision block returns it to the robot for execution. Otherwise, an abort signal is issued.

5 Experiments

This section demonstrates how our causality-based decision-making framework (Sec. 3) enhances the robot's efficiency and safety. In particular, our approach enables the robot to estimate both congestion levels in specific areas of the environment at different times and the battery consumption required for a given task. Estimating congestion allows the robot to anticipate the habitual presence of workers in certain areas at specific times, enabling it to proactively avoid these areas, accommodate human activities, and maintain a safer environment. Additionally, estimating battery consumption helps the robot decide whether to proceed with or abort a task, ensuring it does not risk depleting its battery, failing to complete the assigned task, or being unable to autonomously return to the charging station.

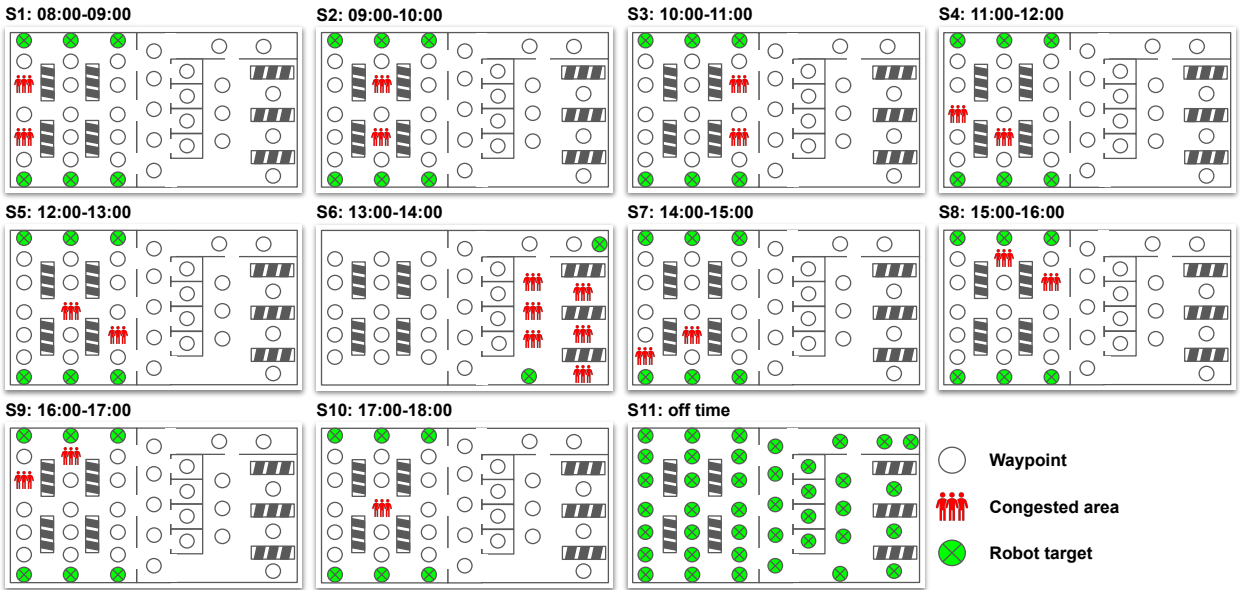

Figure 7: Experimental scenario simulated using our simulator, as described in Sec. 4. The scenario is divided into 11 time slots (S), during which worker congestion areas and robot tasks change dynamically.

5.1 Experimental Setup

Collecting real-world data in a warehouse-like environment with multiple workers and dynamic contextual factors would require significant time and financial resources. Given these constraints, we evaluate our decision-making framework in simulation, similarly to other recent works on multi-agent systems and human-robot social navigation [59, 60]. Our simulator enables the creation of different controlled and repeatable HRSI scenarios, allowing for a systematic analysis of how environmental conditions, agent behaviours, and task constraints influence HRSIs. The data generated by multiple simulated scenarios is processed by our framework to learn a causal model. The latter is finally used to perform actual inference and decision-making, as explained in the following sections.

Simulated Scenarios We designed 11 different scenarios with varying worker congestion areas and robot tasks, as illustrated in Fig. 7. These scenarios correspond to 11 different time slots ($S1$-$S11$) throughout the day, capturing realistic variations in worker activity. At each time slot, we assigned a higher probability for waypoints (Ws) to be occupied by workers. This models the fact that, at different times of the day, workers perform specific tasks in designated areas. For instance, in $S1$–$S5$ and $S7$–$S10$, workers are engaged in normal duties, primarily occupying working areas such as shelves and offices. The slot $S6$ represents lunchtime, during which workers are concentrated in the canteen area. Finally, $S11$ models the off-time period when workers are typically absent. Some congestion areas (represented by a red crowd icon in Fig. 7) correspond to waypoints with the highest probability of being occupied. However, workers are still allowed to move to other locations with lower probabilities, i.e., non-congested areas represented by white circles in Fig. 7. This models the natural behaviour of workers taking breaks, going to the toilet, visiting the canteen, or occasionally moving to other locations beyond their primary working area.

Also the robot's tasks vary depending on the time slot to align with human activities. In $S1$–$S10$ (except $S6$), the robot continuously moves between designated targets (represented as green crossed circles in Fig. 7) at the top and bottom of the working area. Each time, it randomly selects one target from the top and one from the bottom, simulating a pick-and-place task. In $S6$ (lunchtime), the robot assists in the canteen by performing service-related tasks, such as carrying trays or collecting and disposing of waste in bins. The robot's goals in Fig. 7 ($S6$) reflect this scenario: one near the canteen and the other near the entrance. Finally, in $S11$, when workers are no longer in the warehouse, the robot is assigned a cleaning task. During this period, it navigates through all the waypoints, covering the entire workspace. This final time slot serves to validate the behaviour of our decision-making approach in an empty environment, ensuring that it performs identically to the baseline when no human-robot interactions occur.

Data Generation We collected a full-day simulated data, including robot's velocity V, battery level B, and number of people at each waypoint W. Additionally, contextual factors such as the presence of unexpected obstacles O (modelled by red boxes as shown in Fig. 12 top), charging status C, waypoint W, and time slot S were directly extracted from the

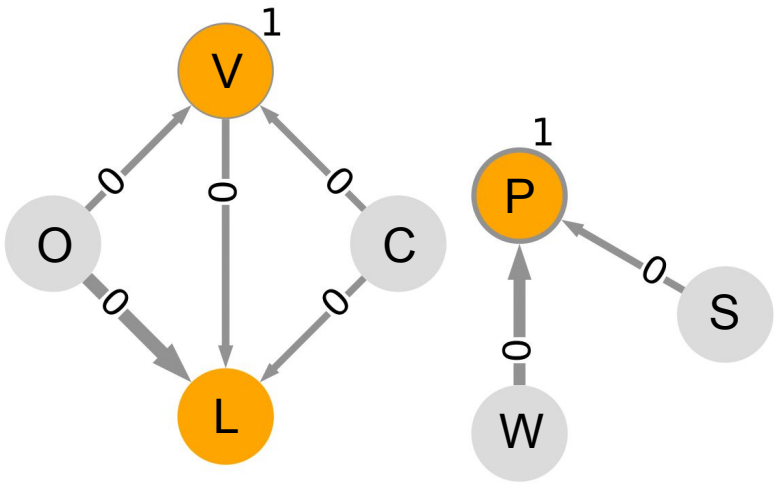

Figure 8: Causal model retrieved from the full scenario. Context variables are shown in grey, while system variables are highlighted in orange. The thickness of the arrows and node borders represents the strength of cross- and auto-causal dependencies, respectively, while the numbers on each node and link indicate the time lag of the dependency.

simulator. We simulated the presence of 50 workers in the warehouse-like scenario, ensuring that their goal selection aligned with the scenario shown in Fig. 7.

We set the obstacle appearance probability to a value of 25%, representing a trade-off between completely obstacle-free environments and highly cluttered ones (e.g., 50% probability). While the latter represents a more challenging scenario, it is unlikely to occur in typical real-world settings. This setup reflects realistic conditions where workers occasionally leave objects–such as boxes, pallets, or forklifts–in corridors or workspaces, thereby affecting the robot's navigation, velocity, and battery discharge dynamics.

We assumed the robot starts with a fully-charged battery and set its parameters to be consistent with its actual lifetime[7] in both idle and motion modes. During this data collection phase, the robot navigated the environment using a ROS-based navigation stack that relies on the A* algorithm as global planner [61, 62], employing the shortest path as its heuristic to reach its goal. This shortest-path strategy serves as a baseline for evaluating our causal decision-making approach, which will be analysed in the following sections.

Data Post-processing To reduce the dataset size and prepare it for our framework's learning pipeline, we first subsampled the recorded data according to the Nyquist–Shannon sampling theorem. We then post-processed the data to derive the necessary variables: the battery consumption variable L was computed from the recorded battery level B, while people density D was derived using Eq. (3), based on the number of people at each waypoint. These transformations allowed us to construct the full set of variables required for causal model learning. Finally, to enable parameter learning, we discretised the post-processed data using the pyAgrum discretiser.

Causal Model Learning The data post-processed in the previous step is then used for causal discovery. We assume an underlying first-order Markov process, and therefore consider a one-step time lag in the causal discovery stage, using J-PCMCI$^+$ to handle context variables.

The reconstructed causal model, shown in Fig. 8, is consistent with the expected causal relationships that describe the full scenario explained in Sec. 4.2 and illustrated in Fig. 5. As anticipated, the causal model consists of two subgraphs: one modelling battery dynamics (left part of the figure) and another capturing people density patterns (right part of the figure). The causal discovery algorithm identified also an additional temporal dependency for the people density $D_{t-1} \rightarrow D_t$ (i.e., an autocorrelation). Although not originally planned, this result is plausible, since congestion levels typically persist over time due to gradual crowd movements. The causal model is then combined with the discretised data to learn the parameters necessary for the inference engine.

5.2 Decision-Making Evaluation Setup

Once built, the model is integrated into the causal inference pipeline of our robot decision-making framework. As explained in Sec. 3.3, the inference pipeline estimates key quantities that guide path selection. Specifically, it employs

the heuristic defined in Eq. (9) to determine a path that balances distance, congestion avoidance, and battery efficiency. Additionally, it enables the robot to decide whether to execute or abort a task based on its battery level. Our causality-based approach is compared against a common shortest-path heuristic for robot navigation [63, 64], which serves as a benchmark.

An experiment is conducted for each time slot S. Workers move according to the waypoint probability distribution defined for S, as shown in Fig. 7. Similarly, the robot performs a predetermined number of tasks, always following the plan outlined in the figure. Regardless of the S duration, each experiment concludes when the robot completes all assigned tasks for that time slot, so that baseline and causal approaches are compared on the same number of tasks rather than the how many tasks the robot manages to complete within S. To eliminate potential biases, each experiment begins with the robot's battery fully charged. Additionally, we predefine the workers' goal sequences to match the scenarios in Fig. 7, ensuring that the only difference between the two approaches is the heuristic used for path planning. We set a 45 seconds deadline for task completion: if the robot fails to complete a task within this time limit, it is considered a failure, and the robot is moved to the next task's starting position. This prevents the robot from being indefinitely stuck due to nearby human presence, while also ensuring that each task starts from the same location for both approaches.

From $S1$ to $S10$, the number of tasks is set to 200 in order to collect enough interaction data for assessing the benefits of D and battery consumption estimations, as well as evaluating the effect of causal decision-making process. In $S11$, when there are no workers, the robot navigates through all the waypoints in the environment, simulating a simple cleaning routine during non-working hours. Each connection between waypoints is considered as a task that the robot must complete. The minimum number of arcs connecting all the waypoints was determined using the Traveling Salesman Problem [65], resulting in 90 connections, corresponding to 90 tasks.

The heuristic uses the following weights: $\lambda_D = 1$, $\lambda_D = 10$, and $\lambda_L = 5$. These values are empirically chosen to avoid congested areas instead of minimising the total travelled distance, so that the robot favors safer and less crowded paths. If the battery drops below a critical threshold (i.e., 20% of the total charge) during the execution of a task, this is considered failed, and the battery is reset to 100%. If the battery falls below the critical threshold after a task has completed, it is still reset but considered a success. Note that for the causal approach, if our decision making framework does not return any valid path to a given goal that satisfies the critical battery constraint, the battery level is set again to 100%, as if the robot had been at the charging station.

5.3 Metrics

Besides principles for social navigation, [66] specifies metrics for their assessment, some of which are used to evaluate the **efficiency** of our approach:

- *Success Rate:* the proportion of successfully completed tasks out of their total number.
- *Failure Rate:* the proportion of failed tasks out of their total number, further categorised into failures due to battery depletion and to congestion.
- *Task Time:* for successful tasks, this metric measures both the time during which the robot is actively moving toward its goal and the time during which it is stalled (i.e., null velocity). For failed tasks, it measures the time wasted without reaching the goal.
- *Travelled Distance:* for successful tasks, this metric quantifies the total distance travelled by the robot, split into planned path length (as computed by the A^* algorithm) and extra distance incurred due to unexpected deviations. For failed tasks, it measures the travel distance wasted without reaching the goal.
- *Battery Usage:* battery consumed during completed tasks or incomplete attempts.

To evaluate the improved **safety** in human-robot shared environments, we considered instead the following metrics:

- *Collision Count:* Measures the number of robot-human collisions, considered as such when the distance between the robot and a person falls below a predefined safety threshold [67]. Specifically, this metric counts instances where a worker enters the robot's circumscribed region[10].
- *Space Compliance:* evaluates the robot's adherence to human spatial preferences based on Hall's proxemic zones [68].

To assess the significance of the differences between our causal approach and the baseline, we apply opportune statistical tests based on the nature of each metric [69]. In particular, for the Success and Failure Rate, we use a Chi-Square test, which is appropriate for categorical outcomes (success vs. failure). For the Collision Count, we employ a Negative

[10] `http://wiki.ros.org/costmap_2d`

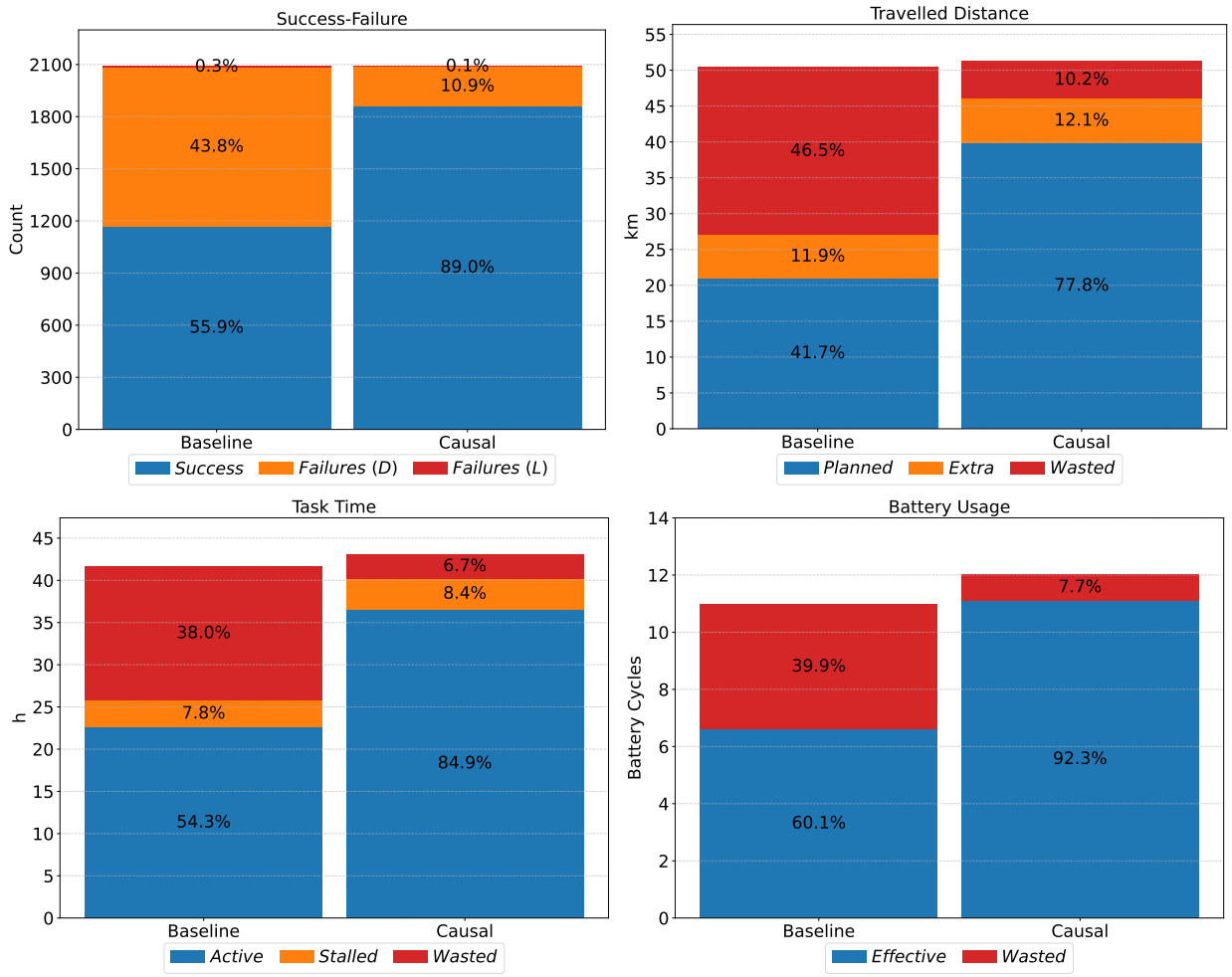

Figure 9: Summary of overall efficiency metrics across all time slots. (Top-left) Task outcomes: (blue) successful tasks, (orange) failures due to high people density D, and (red) failures caused by excessive battery consumption L. (Top-right) Travelled distance breakdown: (blue) planned distance (expected travel), (orange) extra distance (deviations from the expected), and (red) wasted distance linked to failed tasks. (Bottom-left) Task completion time distribution: (blue) active time (robot moving during successful tasks), (orange) stalled time (robot idle in successful tasks), and (red) wasted time (time spent in failed tasks). (Bottom-right) Battery usage analysis: (blue) effective battery consumption in successful tasks and (red) wasted battery in failed tasks.

Binomial test, suitable for count data that exhibits overdispersion (i.e., variance greater than the mean), as observed in our case. For all the other continuous or ordinal metrics—Task Time, Travelled Distance, Battery Usage, and Space Compliance—we use the Mann-Whitney U test, a non-parametric alternative to the t-test, since it does not assume normally distributed data.

5.4 Results

We present the results of our experiments, highlighting the benefits of our approach in in terms of *efficiency* and *safety*.

Efficiency As outlined in Sec. 5.3, the efficiency results shown in Fig. 9 include the following metrics: (top-left) task success and failure counts, (top-right) travelled distance, (bottom-left) task completion time, and (bottom-right) battery consumption. Each graph contains two stacked bars, one for the baseline and one for the causal approach. Each bar is divided into multiple blocks, representing different categories within the same metric. Within each block, the percentage relative to the total height of that bar. This provides a clear visual representation of the proportion of each category within the same bar.

Starting with number of successful and failed tasks (top-left), we distinguish the latter into failures due to the robot getting stuck because of people congestion (orange) and failures caused by the battery level dropping below the critical threshold (red).

The travelled distance (top-right) is also divided into three components: the total planned path length across all time slots (blue), representing the total length of the paths determined by the heuristic; extra travelled distance (orange), which quantifies deviations from the planned paths, computed as the difference between the actual total travelled distance and the total planned distance; and wasted distance (red), corresponding to the distance covered during tasks that ultimately failed. The planned and extra travelled distances are only measured for successfully completed tasks. This metric is shown in kilometers (km).

The task time (bottom-left) is divided into three components: active time (blue), representing the total duration in which the robot is actively moving toward its goal (i.e., performing tasks); stalled time (orange), accounting for periods when the robot stopped due to congestion or obstacle avoidance; and wasted time (red), representing the total time spent on tasks that ultimately resulted in a failure. Note that active and stalled times are only measured for successfully completed tasks. This metric is measured in hours (h).

The battery usage (bottom-right) is divided into two categories: effective battery usage (blue), representing the battery consumed during successfully completed tasks, and wasted battery usage (red), which quantifies the battery consumed in tasks that ultimately resulted in a failure. Battery usage is measured in battery cycles, where one cycle corresponds to consuming 100% of the battery.

Safety Sec. 5.3 defines the metrics to evaluate the safety of HRSI, shown in Fig. 10, and including (left) number of collisions and (right) human-robot proxemic compliance. The number of collisions quantifies instances where robot and human are within contact distance, which is TIAGo's base radius[7]. The graph compares the baseline (blue) and causal (orange) approaches. The right part of Fig. 10 shows a box plot of the distribution of human-robot distances across all time slots. The background highlights different proxemic zones [68]: public (≤ 7.6m, green), social (≤ 3.6m, blue), personal (≤ 1.2m, yellow), and intimate (≤ 0.5m, red).

5.5 Discussions

The results introduced in Sec. 5.4 are discussed here in detail to highlight the benefits of our proposed approach.

Efficiency Fig. 9 (top-left) shows that TIAGo, employing our causality-based decision-making framework, successfully completes 89% of the tasks (1860 out of 2090), compared to only 55.9% for the baseline. This difference is also reflected in the failure rates due to congestion (orange) and battery depletion (red). Specifically, congestion-related failures account for 10.9% in our approach versus 43.8% in the baseline. This demonstrates that the estimations of people density (D) and battery consumption (L) enable the robot to complete nearly 90% of the tasks, whereas the baseline, lacking this knowledge, fails in almost half of the cases. An example of the experiments in Fig. 11 shows a typical scenarios where TIAGo, using our approach, successfully avoids congested areas and completes its task. In contrast, the baseline approach, which prioritises the shortest path—even when it is the busiest—leads the robot into congestion, ultimately causing task failure.

Although the effect is smaller, our approach also improves task-execution decisions based on estimated battery consumption. The causal approach successfully estimates in 7 out of 10 cases whether the battery level is sufficient to complete a task without reaching the critical threshold. In contrast, the baseline approach succeeds only 3 times out of 10, as the robot executes tasks regardless of its battery level and task cost.

The overall distance travelled by the robot is illustrated in Fig. 9 (top-right). The impact of these path selection strategies is evident in the wasted distance (red blocks), which represents the distance travelled in tasks that ultimately failed. The baseline approach, which relies on the shortest-path strategy, results in 46.5% of the total travelled distance being wasted. In contrast, our causality-based approach reduces this to only 10.2%, demonstrating a significantly more efficient motion. The sum of the planned distance (blue) and the extra distance (orange) represents the "effective" distance travelled to complete successful tasks. While the total travelled distance is slightly higher in the causal approach, it enables the robot to use about 90% of the total travelled distance for successful tasks, compared to only 53.6% for the baseline case.

These findings are consistent with the task time results in Fig. 9 (bottom-left). Specifically, the robot actively moves toward its goals for 84.9% of the total working hours using our approach, compared to only 54.3% for the baseline. Moreover, the wasted time—the time spent on tasks that ultimately failed—is drastically reduced from 38% in the baseline to just 6.7% in the causal case.

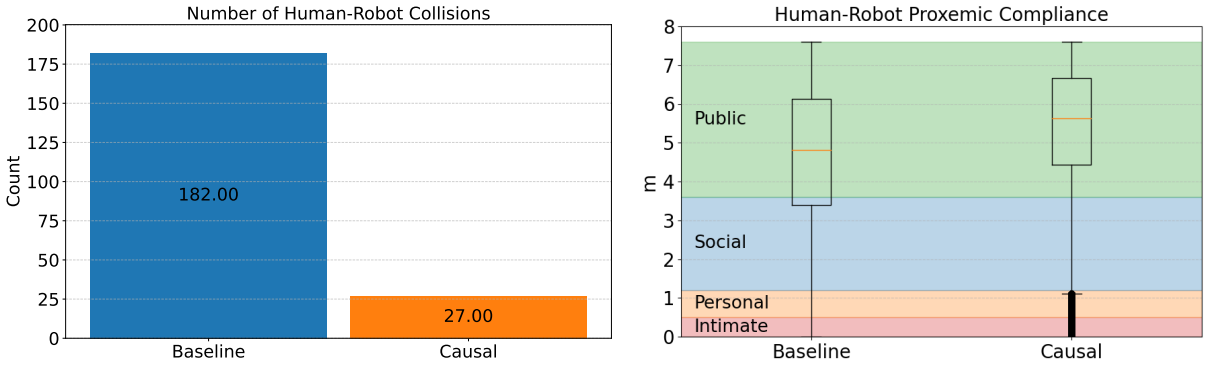

Figure 10: Summary of overall safety results across all time slots. (Left) Number of human-robot collisions: (blue) baseline approach (orange) our approach. (Right) Human-robot proxemic compliance with proxemic zone bands: (green) public, (blue) social, (orange) personal, (red) intimate.

Finally, the battery usage in Fig. 9 (bottom-right) shows that the causal approach requires an almost equivalent number of battery cycles (12 for causal and 11 for baseline), although many more tasks were successfully completed by our approach. Indeed, the battery usage is significantly better managed by the latter, with 92.3% of the battery consumption classified as effective—i.e., spent on tasks that ultimately succeed—while only 7.7% is wasted on failed tasks. In contrast, the baseline approach wasted 39.9% of its battery on failed tasks, which corresponds to more than 4 battery cycles.

Note that, in $S11$ (off-time), both methods behave identically. Specifically, in both the baseline and causal approaches, the robot successfully completes all 90 tasks, travelling comparable distances in the same amount of time and using the same amount of battery. This demonstrates that our approach does not introduce unnecessary path deviations in the absence of workers and congestion.

Statistical significance was confirmed by a Chi-Square test for the success-failure graph and a Mann-Whitney U test for the other metrics, as explained in Sec. 5.3.

Safety Fig. 10 presents the safety-related results. The bar chart (left), which shows the number of times the robot and humans collides, reveals a significant difference between the two approaches. The baseline (blue bar), without information about D and L, relies solely on the shortest-path heuristic. This limitation forces the robot to select the shortest but often busiest path (as shown in Fig. 11), leading to 182 collisions. In contrast, our approach (orange bar), which takes into account people density and battery consumption, leads to only 27 collisions in total.

This observation is further confirmed by the overall distribution of robot-human distances in Fig. 10 (right). This also highlights how both the baseline and causal approaches comply with proxemic zones [68]. In both approaches, the median distance falls within the public zone (green), indicating that on average, the robot maintains a safe distance from humans. However, a key difference emerges when examining the interquartile range (IQR) and lower quantiles. In the baseline approach, the 25th–75th percentile range extends into the social zone (blue), meaning that the robot frequently operates at closer distances to people. More critically, the lower whisker shows that the robot often enters the personal (orange) and intimate (red) zones, indicating also frequent close interactions. Our approach instead maintains the entire IQR within the public zone. The lower whisker and outliers rarely reach the personal and intimate zones, suggesting that close encounters are significantly reduced compared to the baseline. This further highlights the effectiveness of our causality-based decision framework in ensuring that the robot operates at safer distances.

As done for the efficiency, we verified the statistical significance of our results, in this case using a Negative Binomial test for the human-robot collision graph and a Mann-Whitney U test for the proxemic compliance metric.

6 Causal vs Bayesian Inference

Although the advantages of causal inference over a standard Bayesian approach are well established in the literature [48], in this section we demonstrate such benefits through a simplified ablation study focused on our mobile robot's decision-making process.

Figure 11: (Top-left) TIAGo robot with a person in a real-world scenario. (Top-right) TIAGo robot with a simulated agent in PeopleFlow. (Centre and bottom rows) Visualisations of the TIAGo robot executing its assigned tasks in two scenarios: (left) $S2$ working time and (right) $S6$ lunchtime. The robot's goal is represented by a green sphere, while the planned path is highlighted in blue. Congested areas align with Fig. 7 in both scenarios. (centre) Path generated by the shortest-strategy heuristic in the baseline approach. (bottom) Path generated by our approach. The bottom-line graphs illustrate the effectiveness of our method, which prioritises safety over minimising travel distance.

Simplified Scenario In this study we focus only on the estimation of L using the causal inference engine. To simplify the analysis in terms number of variables involved, we do not consider people congestion areas. In this simplified scenario the TIAGo robot navigates between its target positions (diamond symbols in Fig. 4, top) while draining the battery according to the model in (1) in the discharging case ($C = 0$). Additionally, we introduce unexpected obstacles (e.g., red box in Fig. 12 top) that have an impact on robot velocity and battery consumption.

The robot continuously moves between target stations, simulating the delivery of items from trays to conveyors. During task execution, random obstacles appear in its path, with a pre-defined probability. These force the robot to adjust its velocity to avoid collisions and overtake them to complete its task. Once avoided, the obstacle disappears.

We simulate 1 hour of operation, extracting from our simulator V, L, and the binary contextual factor O. We assumed the robot starts with a fully charged battery ($B = 100$) and set the battery parameters by aligning their values with the actual battery lifetime[7] in both idle and motion modes. The recorded time-series is then subsampled and stored by the *data pipeline*, preparing it for the following *learning pipeline*.

The causal model, illustrated in Fig. 12 (bottom-left), is discovered by the J-PCMCI$^+$ algorithm, chosen because of the presence of the context variable O, assuming a first-order Markov process (one time step lag). As expected, the model is essentially a simplified version of the previous one in Fig. 5, restricted to this specific case where only the V, L, and O variables are considered ($L_t \leftarrow C_t \rightarrow V_t$ is missing since we consider only $C = 0$). The final discretised model resulting from the parameter learning step is shown in Fig. 12 (bottom-right).

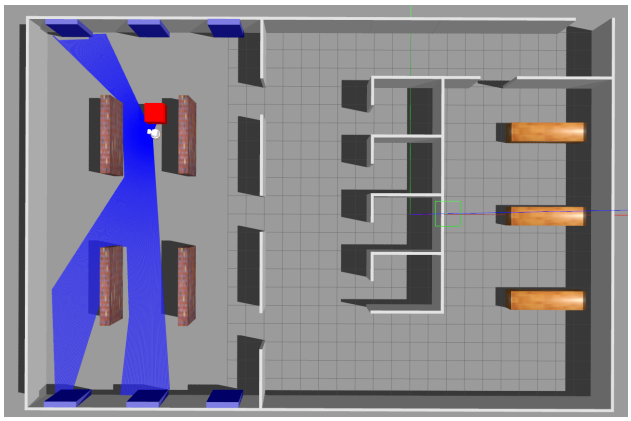

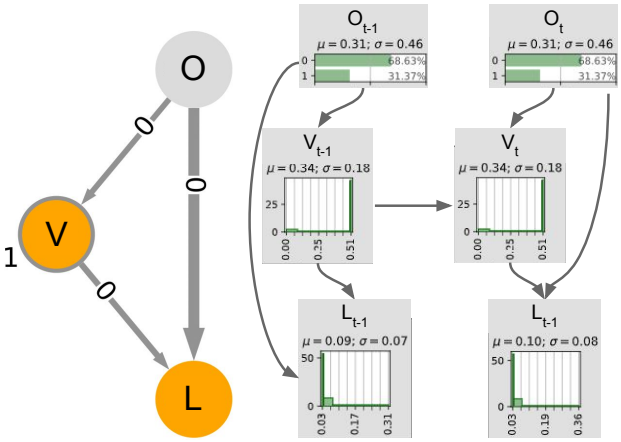

Figure 12: Simplified scenario. (Top) The TIAGo robot navigating between its target positions to complete tasks while avoiding unexpected obstacles (red cubes) in the environment. (Bottom-left) Causal model retrieved from the preliminary study. Context variables are shown in grey, while system variables are highlighted in orange. The thickness of the arrows and node borders represents the strength of cross- and auto-causal dependencies, respectively, while the numbers on each node and link indicate the time lag of the dependency. (Bottom-right) Causal inference engine derived from the built causal model.

Theoretical Analysis When estimating the relationship between two variables in the presence of a confounder, standard Bayesian inference operates purely in an observational setting, modelling the joint probability distribution and updating beliefs based on conditional dependencies. However, Bayesian networks do not distinguish between correlation and causation, making them ineffective when trying to determine the causal impact of one variable on another. This limitation becomes critical when a confounder influences both the treatment and the outcome, introducing spurious associations that bias the estimation. In contrast, causal inference explicitly models interventions using the do-operator, which allows us to estimate the cause-effect while accounting for confounders.

As explained in Sec. 4.1, the factor O represents unexpected static obstacles in the environment, which influence both the robot's velocity V and battery consumption L. This makes O a confounder between these two variables. In our scenario, as outlined in Sec. 3.3, the robot is assigned a task and queries the causal inference engine to make a decision whether to start or abort the task based on its battery level. Hence, an intervention on V is performed to estimate L before the task begins. However, the robot cannot know in advance whether it will encounter an unexpected obstacle along its path. Thus, we cannot directly condition on the confounder O, since its value is unknown at the time of decision-making. As a result, failing to account for this dependency would bias the causal effect estimation. Instead, by adjusting for O, we can isolate the true causal relationship between V and L, ensuring a more accurate estimate of battery consumption in an uncertain scenario.

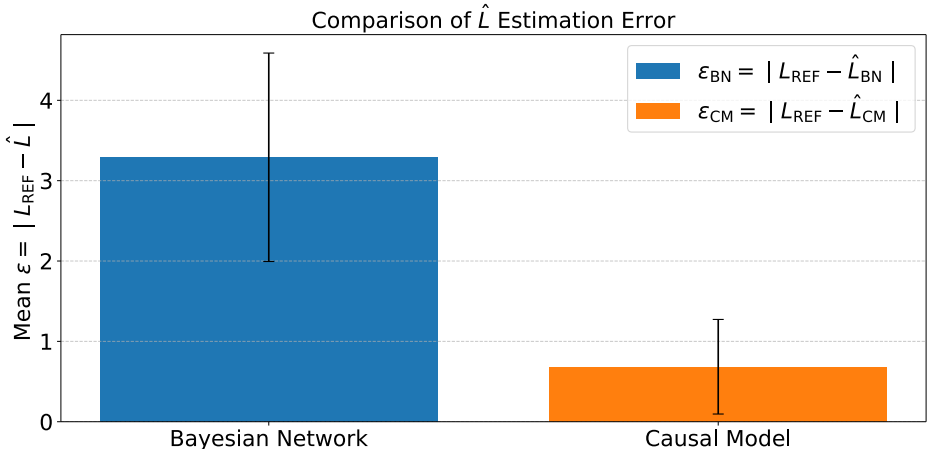

Figure 13: Comparison of the $\hat{L}$ estimation error for the query *"What if the mobile robot covers a distance of 60m at velocity v?"*. The bars represent the MAE across different O probabilities, ranging from 10% to 50%, for the two inference methods: (blue) Bayesian inference and (orange) Causal inference. Error bars indicate the standard deviation of the absolute error.

A typical Bayesian approach would estimate the probability of battery consumption at time t, given a certain robot velocity, applying the law of total probability with conditioning as follows:

$$\mathrm{P}(L_t \mid V_t) = \sum_{O_t} \mathrm{P}(L_t \mid V_t, O_t)\mathrm{P}(O_t \mid V_t) \tag{11}$$

This formulation does not perform any intervention, i.e., it selects a particular V without breaking all the incoming edges. By conditioning on the observed velocity, $\mathrm{P}(O_t \mid V_t)$ implicitly selects specific values of O depending on V. Such indirect selection introduces a confounding bias, since the estimated effect of V on L remains influenced by O.

To correctly estimate the causal effect of V on L, we must apply the do-operator to simulate an intervention:

$$\mathrm{P}(L_t \mid do(V_t)) = \sum_{O_t} \mathrm{P}(L_t \mid V_t, O_t)\mathrm{P}(O_t) \tag{12}$$

The equation is essentially a backdoor adjustment [48], where we account for the confounder O by integrating over its distribution. This removes the confounding bias, yielding an unbiased causal effect of V on L.

Numerical Analysis By simulating numerically a real query, we can better appreciate the difference between the two methods. Consider the following scenario inspired by a typical task assigned to the robot during our experiments presented in Sec. 5: TIAGo is at point A and must deliver an object to point B, with a distance of 60m between them. There is a 30% probability of some unexpected obstacle O obstructing its path during the task. The robot's query is "*what if I cover this distance at my maximum velocity?*". At its maximum velocity—0.5m/s for the TIAGo robot—TIAGo will need $\Delta_t = 120$ seconds to cover the distance, used in (1) to calculate the reference value of L. Since the value of O is unknown at decision time, the correct reference for evaluation is the expected value of L, averaging over the two possible outcomes (i.e., $O = 0$ and $O = 1$). This yields a reference battery consumption of $L_{\text{REF}} = -2.504$, where REF stands for reference. Using Eq. (11) for Bayesian inference and Eq. (12) for causal inference, we estimate the probability distributions of L under conditioning (Bayesian setting) and intervention (causal setting), respectively. By computing the expectation, we obtain the numerical estimates for the Bayesian network $\hat{L}_{\text{BN}} = -1.486$ and causal model $\hat{L}_{\text{CM}} = -2.142$, with the corresponding absolute errors from the reference value are $\epsilon_{BN} = \ | L_{\text{REF}} - \hat{L}_{\text{BN}} | \ = 1.018$ and $\epsilon_{CM} = \ | L_{\text{REF}} - \hat{L}_{\text{CM}} | \ = 0.362$. This shows that the causal model estimates the battery consumption with an error nearly three times smaller than the Bayesian network.

To generalise, we varied the obstacle probability between 10% and 50%, using 10% increments, and compared the two inference methods. Fig. 13 shows the mean absolute error (MAE), for the two inference methods—(blue) Bayesian inference and (orange) Causal inference— across different O probabilities (i.e., 10%, 20%, 30%, 40%, 50%) with error bars representing standard deviations. This comparison demonstrates that, on average, the causal model outperforms the Bayesian network in inference accuracy across the various obstacle probabilities.

7 Conclusion

In this work, we introduced a novel causality-based decision-making framework and a new HRSI simulator featuring a mobile robot, multiple pedestrians, and various contextual factors. These factors influence the dynamics of human and robot's goals, their interactions, and the robot's task execution. Our causality framework integrates data processing, causal discovery, and causal inference, enabling the robot to make better path planning decisions and to determine in advance whether to proceed with or cancel a task. These decisions are based on two causally-inferred quantities: expected people densities in specific areas of the environment, and estimated battery consumption to reach a target location. The proposed system was applied and evaluated in a simulated warehouse scenario with context-dependent goals and interactions, made with PeopleFlow. The results validate the improvements achieved by our solution in terms of planning efficiency and safety for shared human-robot environments.

Building on these results, future work will focus on deploying our approach on a real robot for onboard online decision-making. This step is crucial for evaluating the effectiveness of our method in real-world logistics scenarios involving multiple humans, shared spaces, and complex interactions. Additionally, a promising direction is to enhance our causality-based decision-making framework by integrating a module for causal feature learning (i.e., which variables are important for predicting a certain outcome) into the learning pipeline. Beyond learning the causal structure and parameters, this addition would enable the robot to automatically identify and refine relevant features, enhancing generalisation and adaptability in dynamic environments.

Acknowledgments

This work has received funding from the European Union's Horizon 2020 research and innovation programme under grant agreement No 101017274 (DARKO). GB is also supported by PNRR MUR project PE0000013-FAIR.

References

[1] euRobotics. A unified vision for european robotics: A strategy for innovation, growth and societal impact, December 2024.

[2] National Science Foundation. National Robotics Initiative 3.0: Innovations in Integration of Robotics (NRI-3.0), 2021.

[3] Thomas Hellström. The relevance of causation in robotics: A review, categorization, and analysis. *Paladyn, Journal of Behavioral Robotics*, 12(1):238–255, 2021.

[4] Jake Brawer, Meiying Qin, and Brian Scassellati. A causal approach to tool affordance learning. In *IEEE/RSJ International Conference on Intelligent Robots & Systems (IROS)*, pages 8394–8399, 2020.

[5] Yu Cao, Boyang Li, Qian Li, Adam Stokes, David Ingram, and Aristides Kiprakis. Reasoning operational decisions for robots via time series causal inference. In *2021 IEEE International Conference on Robotics and Automation (ICRA)*, pages 6124–6131, 2021.

[6] Luca Castri, Sariah Mghames, Marc Hanheide, and Nicola Bellotto. Causal discovery of dynamic models for predicting human spatial interactions. In *International Conference on Social Robotics*, pages 154–164. Springer, 2022.

[7] Luca Castri, Sariah Mghames, Marc Hanheide, and Nicola Bellotto. Enhancing causal discovery from robot sensor data in dynamic scenarios. In *2nd Conference on Causal Learning and Reasoning*, 2023.

[8] Garrett Katz, Di Wei Huang, Theresa Hauge, Rodolphe Gentili, and James Reggia. A novel parsimonious cause-effect reasoning algorithm for robot imitation and plan recognition. *IEEE Trans. on Cognitive and Developmental Systems*, 2018.

[9] Daniel Angelov, Yordan Hristov, and Subramanian Ramamoorthy. Using causal analysis to learn specifications from task demonstrations. In *Proceedings of the 18th International Conference on Autonomous Agents and MultiAgent Systems, AAMAS*, pages 1341–1349, 2019.

[10] Tabitha E. Lee, Jialiang Alan Zhao, Amrita S. Sawhney, Siddharth Girdhar, and Oliver Kroemer. Causal reasoning in simulation for structure and transfer learning of robot manipulation policies. In *2021 IEEE International Conference on Robotics and Automation (ICRA)*, pages 4776–4782, 2021.

[11] Ricardo Cannizzaro, Jonathan Routley, and Lars Kunze. Towards a causal probabilistic framework for prediction, action-selection & explanations for robot block-stacking tasks. In *IEEE/RSJ International Conference on Intelligent Robots & Systems (IROS) Workshop on Causality for Robotics*. IEEE, 2023.

[12] Ricardo Cannizzaro, Rhys Howard, Paulina Lewinska, and Lars Kunze. Towards probabilistic causal discovery, inference & explanations for autonomous drones in mine surveying tasks. In *IEEE/RSJ International Conference on Intelligent Robots & Systems (IROS) Workshop on Causality for Robotics*. IEEE, 2023.

[13] Ricardo Cannizzaro and Lars Kunze. Car-despot: Causally-informed online pomdp planning for robots in confounded environments. In *IEEE/RSJ International Conference on Intelligent Robots & Systems (IROS)*. IEEE, October 2023.

[14] Tamlin Love, Antonio Andriella, and Guillem Alenyà. What would i do if. . . ? promoting understanding in hri through real-time explanations in the wild. In *2024 33rd IEEE International Conference on Robot and Human Interactive Communication (ROMAN)*, pages 504–509. IEEE, 2024.

[15] Tamlin Love, Antonio Andriella, and Guillem Alenyà. Towards explainable proactive robot interactions for groups of people in unstructured environments. In *Companion of the 2024 ACM/IEEE International Conference on Human-Robot Interaction*, pages 697–701, 2024.

[16] Clark Glymour, Kun Zhang, and Peter Spirtes. Review of causal discovery methods based on graphical models. *Frontiers in genetics*, 10:524, 2019.

[17] Charles K Assaad, Emilie Devijver, and Eric Gaussier. Survey and evaluation of causal discovery methods for time series. *Journal of Artificial Intelligence Research*, 73:767–819, 2022.

[18] Peter Spirtes, Clark N Glymour, and Richard Scheines. *Causation, prediction, and search*. MIT press, 2000.

[19] Jakob Runge. Causal network reconstruction from time series: From theoretical assumptions to practical estimation. *Chaos: An Interdisciplinary Journal of Nonlinear Science*, 28(7), 2018.

[20] Jakob Runge, Peer Nowack, Marlene Kretschmer, Seth Flaxman, and Dino Sejdinovic. Detecting and quantifying causal associations in large nonlinear time series datasets. *Science advances*, 5(11):eaau4996, 2019.

[21] Supat Saetia, Natsue Yoshimura, and Yasuharu Koike. Constructing brain connectivity model using causal network reconstruction approach. *Frontiers in Neuroinformatics*, 15:619557, 2021.

[22] Jakob Runge. Discovering contemporaneous and lagged causal relations in autocorrelated nonlinear time series datasets. In *Conference on Uncertainty in Artificial Intelligence (UAI)*, pages 1388–1397. PMLR, 2020.

[23] Wiebke Günther, Urmi Ninad, and Jakob Runge. Causal discovery for time series from multiple datasets with latent contexts. In Robin J. Evans and Ilya Shpitser, editors, *Proceedings of the Thirty-Ninth Conference on Uncertainty in Artificial Intelligence*, volume 216 of *Proceedings of Machine Learning Research*, pages 766–776. PMLR, 31 Jul–04 Aug 2023.

[24] Andreas Gerhardus and Jakob Runge. High-recall causal discovery for autocorrelated time series with latent confounders. *Advances in Neural Information Processing Systems*, 33:12615–12625, 2020.

[25] Luca Castri, Sariah Mghames, Marc Hanheide, and Nicola Bellotto. Candoit: Causal discovery with observational and interventional data from time series. *Advanced Intelligent Systems*, 6(12):2400181, 2024.

[26] Luca Castri, Gloria Beraldo, Sariah Mghames, Marc Hanheide, and Nicola Bellotto. Experimental evaluation of ros-causal in real-world human-robot spatial interaction scenarios. In *2024 33rd IEEE International Conference on Robot and Human Interactive Communication (ROMAN)*, pages 1603–1609, 2024.

[27] Debasmita Mukherjee, Kashish Gupta, Li Hsin Chang, and Homayoun Najjaran. A survey of robot learning strategies for human-robot collaboration in industrial settings. *Robotics and Computer-Integrated Manufacturing*, 73:102231, 2022.

[28] Juan P Vasconez, George A Kantor, and Fernando A Auat Cheein. Human–robot interaction in agriculture: A survey and current challenges. *Biosystems engineering*, 179:35–48, 2019.

[29] Roohollah Jahanmahin, Sara Masoud, Jeremy Rickli, and Ana Djuric. Human-robot interactions in manufacturing: A survey of human behavior modeling. *Robotics and Computer-Integrated Manufacturing*, 78:102404, 2022.

[30] Abhinav Dahiya, Alexander M Aroyo, Kerstin Dautenhahn, and Stephen L Smith. A survey of multi-agent human–robot interaction systems. *Robotics and Autonomous Systems*, 161:104335, 2023.

[31] Christian Dondrup, Nicola Bellotto, Marc Hanheide, Kerstin Eder, and Ute Leonards. A computational model of human-robot spatial interactions based on a qualitative trajectory calculus. *Robotics*, 4(1):63–102, 2015.

[32] Sariah Mghames, Luca Castri, Marc Hanheide, and Nicola Bellotto. A neuro-symbolic approach for enhanced human motion prediction. In *2023 International Joint Conference on Neural Networks (IJCNN)*, pages 1–8. IEEE, 2023.

[33] Sariah Mghames, Luca Castri, Marc Hanheide, and Nicola Bellotto. Qualitative prediction of multi-agent spatial interactions. In *2023 32nd IEEE International Conference on Robot and Human Interactive Communication (RO-MAN)*, pages 1170–1175. IEEE, 2023.

[34] Y. Liu, R. Cadei, J. Schweizer, S. Bahmani, and A. Alahi. Towards robust and adaptive motion forecasting: A causal representation perspective. In *Proceedings of the IEEE/CVF Conference on Computer Vision and Pattern Recognition (CVPR)*, pages 17081–17092, 2022.

[35] Andrey Rudenko, Tomasz P Kucner, Chittaranjan S Swaminathan, Ravi T Chadalavada, Kai O Arras, and Achim J Lilienthal. Thör: Human-robot navigation data collection and accurate motion trajectories dataset. *IEEE Robotics & Automation Letters*, pages 676–682, 2020.

[36] Tim Schreiter, Tiago Rodrigues de Almeida, Yufei Zhu, Eduardo Gutierrez Maestro, Lucas Morillo-Mendez, Andrey Rudenko, Luigi Palmieri, Tomasz P Kucner, Martin Magnusson, and Achim J Lilienthal. Thör-magni: A large-scale indoor motion capture recording of human movement and robot interaction. *The International Journal of Robotics Research*, page 02783649241274794, 2024.

[37] Dražen Brščić, Takayuki Kanda, Tetsushi Ikeda, and Takahiro Miyashita. Person tracking in large public spaces using 3-d range sensors. *IEEE Trans. on Human-Machine Systems*, pages 522–534, 2013.

[38] Roberto Martin-Martin, Mihir Patel, Hamid Rezatofighi, Abhijeet Shenoi, JunYoung Gwak, Eric Frankel, Amir Sadeghian, and Silvio Savarese. Jrdb: A dataset and benchmark of egocentric robot visual perception of humans in built environments. *IEEE transactions on pattern analysis and machine intelligence*, 2021.

[39] Nathan Tsoi, Alec Xiang, Peter Yu, Samuel S. Sohn, Greg Schwartz, Subashri Ramesh, Mohamed Hussein, Anjali W. Gupta, Mubbasir Kapadia, and Marynel Vázquez. Sean 2.0: Formalizing and generating social situations for robot navigation. *IEEE Robotics and Automation Letters*, pages 1–8, 2022.

[40] Anoop Aroor, Susan L Epstein, and Raj Korpan. Mengeros: A crowd simulation tool for autonomous robot navigation. In *AAAI Fall Symposia*, pages 123–125, 2017.

[41] Changan Chen, Yuejiang Liu, Sven Kreiss, and Alexandre Alahi. Crowd-robot interaction: Crowd-aware robot navigation with attention-based deep reinforcement learning. In *2019 international conference on robotics and automation (ICRA)*, pages 6015–6022. IEEE, 2019.

[42] Jarrett Holtz and Joydeep Biswas. Socialgym: A framework for benchmarking social robot navigation. In *2022 IEEE/RSJ International Conference on Intelligent Robots and Systems (IROS)*, pages 11246–11252. IEEE, 2022.

[43] Judea Pearl and Dana Mackenzie. *The book of why: the new science of cause and effect*. Basic books, 2018.

[44] Elena S Dimitrova, M Paola Vera Licona, John McGee, and Reinhard Laubenbacher. Discretization of time series data. *Journal of Computational Biology*, 17(6):853–868, 2010.

[45] Pratap Dangeti. *Statistics for machine learning*. Packt Publishing Ltd, 2017.

[46] Anna K Raichev, Jin Tian, Alexander Ihler, and Rina Dechter. Estimating causal effects from learned causal networks. In *9th Causal Inference Workshop at UAI 2024*, 2024.

[47] In Jae Myung. Tutorial on maximum likelihood estimation. *Journal of mathematical Psychology*, 47(1):90–100, 2003.

[48] Judea Pearl. *Causality*. Cambridge university press, 2009.

[49] Gaspard Ducamp, Christophe Gonzales, and Pierre-Henri Wuillemin. agrum/pyagrum: a toolbox to build models and algorithms for probabilistic graphical models in python. In *International Conference on Probabilistic Graphical Models*. PMLR, 2020.

[50] Luca Castri, Gloria Beraldo, Sariah Mghames, Marc Hanheide, and Nicola Bellotto. Ros-causal: A ros-based causal analysis framework for human-robot interaction applications. In *Workshop on Causal Learning for Human-Robot Interaction (Causal-HRI), ACM/IEEE International Conference on Human-Robot Interaction (HRI)*, 2024.

[51] Dirk Helbing and Peter Molnar. Social force model for pedestrian dynamics. *Physical review E*, 51(5):4282, 1995.

[52] Goran Dukic and Tihomir Opetuk. Warehouse layouts. In *Warehousing in the Global Supply Chain: Advanced Models, Tools and Applications for Storage Systems*, pages 55–69. Springer, 2012.

[53] Milan Tomy, Bruno Lacerda, Nick Hawes, and Jeremy L Wyatt. Battery charge scheduling in long-life autonomous mobile robots. In *2019 European Conference on Mobile Robots (ECMR)*, pages 1–6. IEEE, 2019.

[54] Milan Tomy, Bruno Lacerda, Nick Hawes, and Jeremy L Wyatt. Battery charge scheduling in long-life autonomous mobile robots via multi-objective decision making under uncertainty. *Robotics and Autonomous Systems*, 133:103629, 2020.

[55] Giuseppe Fragapane, Rene De Koster, Fabio Sgarbossa, and Jan Ola Strandhagen. Planning and control of autonomous mobile robots for intralogistics: Literature review and research agenda. *European Journal of Operational Research*, 294(2):405–426, 2021.

[56] Elisa Tosello, Paolo Bonel, Alberto Buranello, Marco Carraro, Alessandro Cimatti, Lorenzo Granelli, Stefan Panjkovic, and Andrea Micheli. Opportunistic (re) planning for long-term deep-ocean inspection: An autonomous underwater architecture. *IEEE Robotics & Automation Magazine*, 2024.

[57] Linfei Hou, Liang Zhang, and Jongwon Kim. Energy modeling and power measurement for mobile robots. *Energies*, 12(1):27, 2018.

[58] Thomas Meneweger, Daniela Wurhofer, Verena Fuchsberger, and Manfred Tscheligi. Factory workers' ordinary user experiences: An overlooked perspective. *Human Technology*, 14(2):209–232, 2018.

[59] Christoforos I Mavrogiannis and Ross A Knepper. Multi-agent path topology in support of socially competent navigation planning. *The International Journal of Robotics Research*, 38(2-3):338–356, 2019.

[60] Christoforos Mavrogiannis and Ross A Knepper. Hamiltonian coordination primitives for decentralized multiagent navigation. *The International Journal of Robotics Research*, 40(10-11):1234–1254, 2021.

[61] Eitan Marder-Eppstein, Eric Berger, Tully Foote, Brian Gerkey, and Kurt Konolige. The office marathon: Robust navigation in an indoor office environment. In *2010 IEEE international conference on robotics and automation*, pages 300–307. IEEE, 2010.

[62] Hongzhang Zheng, Min Dai, Zhisheng Zhang, Zhijie Xia, Guifu Zhang, and Fang Jia. The navigation based on hybrid a star and teb algorithm implemented in obstacles avoidance. In *2023 29th International Conference on Mechatronics and Machine Vision in Practice (M2VIP)*, pages 1–6. IEEE, 2023.

[63] Chee Sheng Tan, Rosmiwati Mohd-Mokhtar, and Mohd Rizal Arshad. A comprehensive review of coverage path planning in robotics using classical and heuristic algorithms. *IEEE Access*, 9:119310–119342, 2021.

[64] Andreas C Nearchou. Path planning of a mobile robot using genetic heuristics. *Robotica*, 16(5):575–588, 1998.

[65] Gregory Gutin and Abraham P Punnen. *The traveling salesman problem and its variations*, volume 12. Springer Science & Business Media, 2006.

[66] Anthony Francis, Claudia Perez-D'Arpino, Chengshu Li, Fei Xia, Alexandre Alahi, Rachid Alami, Aniket Bera, Abhijat Biswas, Joydeep Biswas, Rohan Chandra, Hao-Tien Lewis Chiang, Michael Everett, Sehoon Ha, Justin Hart, Jonathan P. How, Haresh Karnan, Tsang-Wei Edward Lee, Luis J. Manso, Reuth Mirksy, Soeren Pirk, Phani Teja Singamaneni, Peter Stone, Ada V. Taylor, Peter Trautman, Nathan Tsoi, Marynel Vazquez, Xuesu Xiao, Peng Xu, Naoki Yokoyama, Alexander Toshev, and Roberto Martin-Martin. Principles and guidelines for evaluating social robot navigation algorithms. *ACM Transactions in Human-Robot Interaction*, pages 1–63, 2024.

[67] Christoforos Mavrogiannis, Francesca Baldini, Allan Wang, Dapeng Zhao, Pete Trautman, Aaron Steinfeld, and Jean Oh. Core challenges of social robot navigation: A survey. *ACM Transactions on Human-Robot Interaction*, 12(3):1–39, 2023.

[68] Edward T Hall, Ray L Birdwhistell, Bernhard Bock, Paul Bohannan, A Richard Diebold Jr, Marshall Durbin, Munro S Edmonson, JL Fischer, Dell Hymes, Solon T Kimball, et al. Proxemics [and comments and replies]. *Current anthropology*, 9(2/3):83–108, 1968.

[69] Sophia Rabe-Hesketh and Brian Everitt. *Handbook of statistical analyses using Stata*. CRC Press, 2003.